Mean sea-level variability along the northeast American Atlantic coast and the roles of the wind and the overturning circulation

Philip L. Woodworth[1], Miguel Á. Morales Maqueda[1], Vassil M. Roussenov[2], Richard G. Williams[2], and Chris W. Hughes[1,2]

[1]National Oceanography Centre, Liverpool, United Kingdom, [2]School of Environmental Sciences, University of Liverpool, Liverpool, United Kingdom

Abstract The variability in mean sea level (MSL) during 1950–2009 along the northeast American Atlantic coast north of Cape Hatteras has been studied, using data from tide gauges and satellite altimetry and information from the Liverpool/Hadley Centre (LHC) ocean model, thereby providing new insights into the spatial and temporal scales of the variability. Although a relationship between sea level and the overturning circulation can be identified (an increase of approximately 1.5 cm in MSL for a decrease of 1 Sv in overturning transport), it is the effect of the nearshore wind forcing on the shelf that is found to dominate the interannual sea-level variability. In particular, winds are found to be capable of producing low-frequency changes in MSL ("accelerations") in a narrow coastal band, comparable to those observed by the tide gauges. Evidence is presented supporting the idea of a "'common mode" of spatially coherent low-frequency MSL variability, both to the north and south of Cape Hatteras and throughout the northwest Atlantic, which is associated with large spatial-scale density changes from year to year.

1. Introduction

This paper discusses the interannual variability in mean sea level (MSL) along the northeast American Atlantic coast north of Cape Hatteras (35°N). At this point, the western boundary current of the Gulf Stream departs from the coast, to become eventually the North Atlantic Drift [*Stewart*, 2008]. North of the Cape is a wide shelf with variable bathymetry, notably in the Gulf of Maine, where the deeper waters of the Gulf are separated from the open sea by Georges Bank.

A long-standing challenge for this area has been to determine the relative importance to MSL variability of several processes. One process concerns along-shore wind stress acting on the shallow waters of the wide continental shelf, as discussed by *Sandstrom* [1980], *Csanady* [1982], *Thompson* [1986], and others. Recently, *Andres et al.* [2013] found significant correlations for the period 1970–2012 between annual MSL at stations north of Cape Hatteras and along-shore wind stress on the Scotian Shelf and in the Gulf of Maine. However, they concluded that other, more remote processes could not be excluded as additional contributors to MSL variability. Their study made no use of ocean models.

A second process concerns variability in Gulf Stream or Atlantic Meridional Overturning Circulation (MOC) strength. A "fingerprint" of a weakening MOC could be provided by steric changes and mass redistributions in the shelf and continental slope areas of the NW Atlantic, resulting in an increase in MSL along this coastline. This possibility was suggested by *Bingham and Hughes* [2009] using an ocean model and has been further studied with the use of climate models [*Yin et al.*, 2009; *Yin and Goddard*, 2013]. *Sallenger et al.* [2012] and *Boon* [2012] considered the possibility of an MOC fingerprint in their discussions of a positive acceleration in MSL since the mid-1980s for stations north of Cape Hatteras.

A third process, not necessarily independent of the other two, concerns a "common mode" of spatially coherent MSL variability along the western North Atlantic, Gulf of Mexico, and Caribbean coastlines that *Thompson and Mitchum* [2014] concluded was primarily due to divergence of Sverdrup transport in the basin interior east of the 65°W meridian resulting in net zonal flows across the meridian, consistent with previous findings by *Hong et al.* [2000]. However, there are also known to be major differences in variability

throughout the region. This applies especially to stations north and south of Cape Hatteras [e.g., *Thompson*, 1986]. Many other papers can be found in the literature that discuss patterns of sea level change that result from ocean circulation variability [e.g., *Häkkinen*, 2001; *van der Schrier et al.*, 2004; *Levermann et al.*, 2005; *Frankcombe and Dijkstra*, 2009; *Lorbacher et al.*, 2010], but for the present paper we shall focus on the three processes mentioned above.

We have made use of data sets provided by tide gauges and a global ocean model for the period 1950–2009, and also by altimetry since 1993, to investigate further the magnitude and source of coastal MSL interannual variability north of Cape Hatteras, and the particular roles of the wind and the overturning circulation. These data sets are described in section 2. In section 3, we consider the coherence of MSL variability along the coast and across the shelf to the deep ocean, both in the observed MSL data and in the ocean model. We discuss the role of the wind in initiating MSL variability, and the low-amplitude variability that results without wind forcing. That leads to consideration of the role of the MOC in MSL variability and also that of the "common mode." In section 4, we investigate whether the local wind forcing along the shelf and slope can also be an important contributor to observed long-term accelerations in MSL. Section 5 discusses further the role of the wind in initiating coastal MSL variability, using idealized models independent of our main ocean model. Our conclusions are summarized in section 6.

2. Data Sets and Models

The northeast American coastline has many MSL records spanning most of the 20th century obtained from well-maintained tide gauges [*DFO*, 2014; *NOAA*, 2014]. All tide gauge MSL data were obtained from the Permanent Service for Mean Sea Level (PSMSL) [*Holgate et al.*, 2012, www.psmsl.org]. Annual MSL values were adjusted for the local inverse barometer effect using sea level air pressures from the National Centers for Environmental Prediction (NCEP)—National Center for Atmospheric Research (NCAR) reanalyses [*Kalnay et al.*, 1996; *Kistler et al.*, 2001, www.cdc.noaa.gov]. A minor correction was made to remove the equilibrium lunar nodal tide (18.61 year period) from the measured MSL; this long-period tide has an amplitude of only several mm along this coastline and is zero at Cape Hatteras [*Woodworth*, 2012]. The pole tide (approximately 14 months period) should in principle also be removed, as its equilibrium response peaks at 45°N with approximately 5 mm amplitude [*Pugh and Woodworth*, 2014]. However, using annual MSLs will reduce any pole tide signal to the mm level or below, albeit aliased through the record.

Altimeter sea levels were obtained from the "reference" series of missions (TOPEX/Poseidon and the Jason series) in quarter-degree gridded form from Archivage, Validation et Interprétation de données des Satellites Océanographiques (AVISO, www.aviso.oceanobs.com). These sea levels are provided with inverse barometer, tidal, and all other instrumental and environmental corrections applied.

Our main ocean model is the Liverpool University implementation of the Massachusetts Institute of Technology (MIT) general circulation model [*Marshall et al.*, 1997a, 1997b] (henceforth called the LHC model, [*Williams et al.*, 2014]), which is constrained by hydrographic fields provided by the UK Met Office/Hadley Centre [*Smith and Murphy*, 2007] and forced by NCEP monthly mean wind stresses. The model has been run on a $1/5 \times 1/6°$ (longitude × latitude) grid with 23 levels in the vertical for the period 1950–2009. A 1° grid version of the model run over the same period has been used for additional diagnostics. The model is ideal for the present study as it adjusts dynamically only in response to the hydrographic information and wind forcing, and does not, as in free models, contain long-term drifts due to the uncertainty in the surface heat and freshwater fluxes.

Interpretation of the LHC model results was aided by analysis of NCEP monthly mean wind stresses (http://www.esrl.noaa.gov/psd/data/gridded/data.ncep.reanalysis.derived.surfaceflux.html). Longer-term information on wind stress was obtained from the 20th Century Reanalysis Project (20CR) [*Compo et al.*, 2011, http://www.esrl.noaa.gov/psd/data/gridded/data.20thC_ReanV2.html]. The 20CR assimilates surface air pressure reports only, and so might be expected to provide less accurate wind fields than NCEP in recent years. However, it has an advantage of providing a consistent data set over a longer period.

3. MSL Variability at the Coast and on the Shelf

3.1. Tide Gauge and Altimeter Data

Tide gauges have the longest records for study of MSL variability on the continental shelf. Figure 1 and Table 1 show the locations of some of the longer records from north of Cape Hatteras, grouped into three
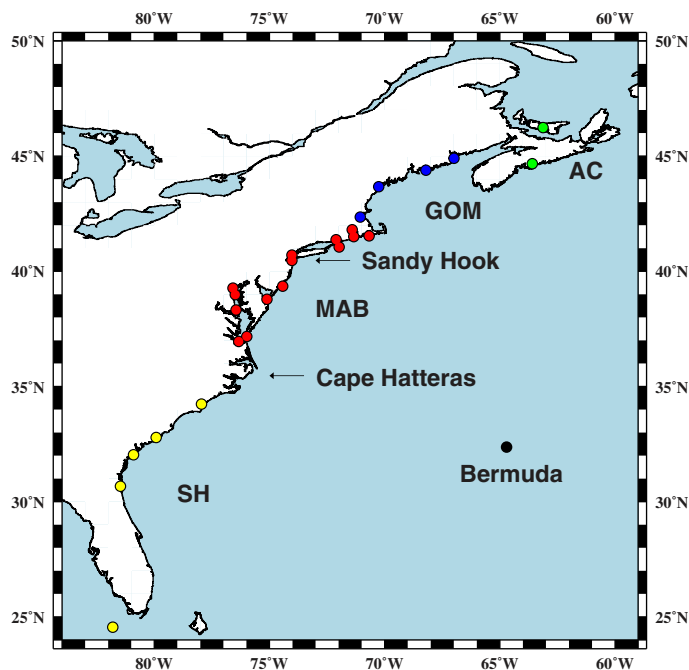
Figure 1. Locations of selected stations in each group: South of Cape Hatteras (SH, yellow), Middle Atlantic Bight (MAB, red), Gulf of Maine (GOM, blue), and Atlantic Canada (AC, green). See Table 1 for a list of the stations shown. Sandy Hook is referred to several times in the text.

sections of coastline (Middle Atlantic Bight (MAB), Gulf of Maine (GOM), and Atlantic Canada (AC)). Stations were selected that have at least 50 years of data for the period 1950 onwards. Also included are five stations from south of Cape Hatteras (SH). Unfortunately, with our requirement for near-complete records, there is a large gap in coverage along the Florida coastline (even with the shorter Mayport and Miami Beach PSMSL records added, there would still be a significant gap). Nevertheless, the five stations provide sufficient information for comparison to those in the north.

Figure 2 (black dots) contains a compilation of the records from north of Cape Hatteras, with in each case an average value and linear trend removed (a similar

Table 1. Tide Gauge Stations Included in the Analysis and Shown in Figure 1

| Station Number	PSMSL Station Code	Station Name	East Longitude	Latitude
South of Cape Hatteras				
1	940071	Key West	−81.807	24.555
2	960021	Fernandina Beach	−81.465	30.672
3	960031	Fort Pulaski	−80.902	32.033
4	960041	Charleston	−79.925	32.782
5	960060	Wilmington	−77.953	34.227
Middle Atlantic Bight				
6	960071	Sewells Point, Hampton Roads	−76.333	36.950
7	960078	Solomon's Island (Biological Laboratory)	−76.450	38.317
8	960080	Annapolis (Naval Academy)	−76.483	38.983
9	960081	Baltimore	−76.583	39.267
10	960083	Kiptopeke Beach	−75.983	37.167
11	960085	Lewes (Breakwater Harbor)	−75.100	38.783
12	960091	Atlantic City	−74.417	39.350
13	960101	Sandy Hook	−74.017	40.467
14	960121	New York (The Battery)	−74.017	40.700
15	960135	Montauk	−71.967	41.050
16	960151	New London	−72.100	41.367
17	960158	Providence (State Pier)	−71.400	41.800
18	960161	Newport	−71.333	41.500
19	960165	Woods Hole Oceanographic Institution	−70.667	41.533
Gulf of Maine				
20	960171	Boston	−71.050	42.350
21	960181	Portland (Maine)	−70.250	43.667
22	960191	Bar Harbor, Frenchman Bay	−68.200	44.383
23	960201	Eastport	−66.983	44.900
Atlantic Canada				
24	970011	Halifax	−63.583	44.667
25	970031	Charlottetown	−63.117	46.233
Bermuda				
26	950011	Bermuda	−64.703	32.373
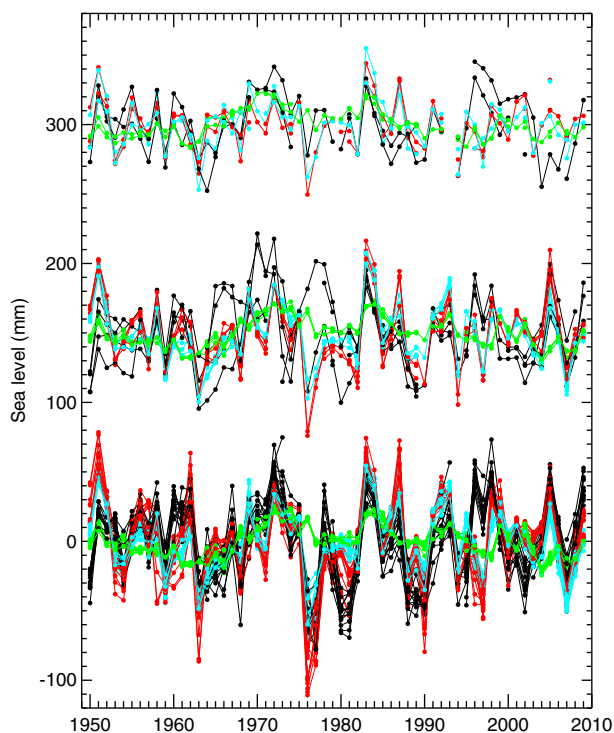
Figure 2. Twenty MSL records from north of Cape Hatteras with at least 50 years of data for the period 1950-on (black points). Each one has been detrended over the period 1950–2009 and corrected for the inverse barometer effect and the equilibrium lunar nodal tide. They are grouped into MAB (bottom), GOM (middle), and AC (top) with offsets for presentation purposes. Other points are from the LHC model higher resolution version (red), 1-degree version (light blue), and 1-degree version without wind forcing (green), similarly detrended.

figure is provided by *Andres et al.* [2013]). MSL can be seen to vary by ± 50 mm on a typically decadal timescale, with the individual records in each section of coastline being very similar. The main exception concerns the four stations in the GOM during the late 1960s and 1970s, with differences of more than 50 mm between the two southern, complete records (Boston and Portland), the two northern records (Bar Harbor and Eastport) having several gaps in this period.

MSL variability is coherent at interannual timescales *along* the coast, as can be inferred from Figure 2. Figure 3 shows that (zero-lag) correlation coefficients between pairs of records north of Cape Hatteras are always high, dropping to about 0.4 between stations most distant apart. Maximum correlation is obtained for stations in the central MAB, and between those stations and others further south toward Cape Hatteras, rather than toward the north and Nova Scotia. Aside from the oceanographic interpretation that Figure 3 provides, the high correlations demonstrate the quality of historical tide gauge recording in this region.

Figure 3 also demonstrates how different régimes of MSL variability exist at stations north and south of Cape Hatteras (stations 6–25 and 1–5 respectively), with separate groupings of higher correlation. *Mitchum* [2011] has shown that records from stations in the Gulf of Mexico and SE United States as far north as Cape Hatteras demonstrate their own regional coherence.

The spatial scales of interannual variability in MSL *across* the shelf and in the nearby deep ocean can be studied with the AVISO altimeter data. In each grid box, the weekly anomalies of sea level were averaged into yearly means and detrended over the period 1993–2009. (This period was chosen for comparison to model findings below, 2009 being the end of the model run. A similar figure is obtained including the latest available altimeter data.) Figure 4a shows the standard deviation of the annual variability to have large values in deep waters toward the Gulf Stream and near the coasts of the MAB and GOM, but not so much around the AC coast, separated by a band of lower variability at the shelf edge (see also *Andres et al.* [2013], Figure 2b). One has always to be wary of using altimetry near the coast, owing to the larger uncertainties in tidal and other corrections in coastal areas [*Vignudelli et al.*, 2011]. Nevertheless, in this case, the altimeter variability along the coast is plausible, being coherent across most of the shelf (Figure 4b), as known from previous studies [e.g., *Bingham and Hughes*, 2009], and highly correlated with that measured at the coast itself by tide gauges (Figure 4c of *Andres et al.* [2013]).

3.2. MSL Variability in the LHC Model
The pattern of standard deviations of annual MSL from the LHC model during this period (Figure 5) has some similarity to that from the altimetry (Figure 4a), in that a gentle variability minimum separates regions of higher coastal and shelf variability in the MAB and GOM from the higher deep-ocean variability. However, the coastal variability in the model is tighter to the coast than for the altimetry and the band of low
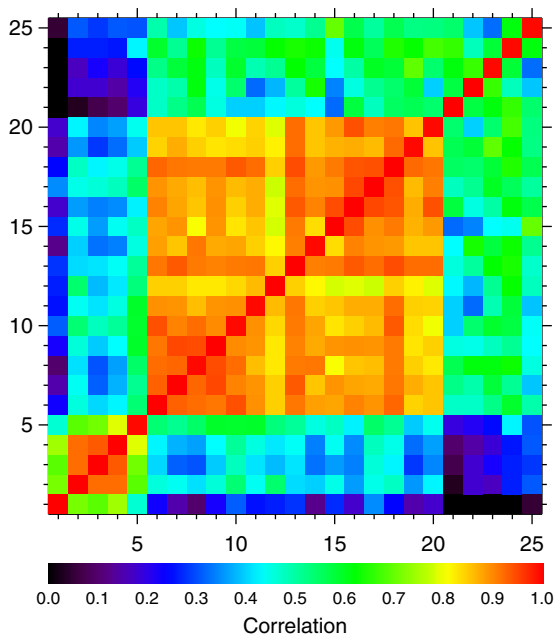
Figure 3. Correlations between MSL values at pairs of stations shown in Figure 1 and Table 1. Stations 1–5 are south of Cape Hatteras. Stations 6–19, 20–23, and 24–25 are in the Middle Atlantic Bight, Gulf of Maine, and Atlantic Canada, respectively.

variability near the shelf edge is wider. In addition, the model has lower variability in the central gyre (see below). Figure 5 is almost the same as that for the entire model run 1950–2009 (supporting information Figure S1). In both model and altimetry, the coastal variability is lower for the Atlantic Canada coast than for the Middle Atlantic Bight and Gulf of Maine. Overall, we conclude that the model does a reasonable qualitative job of explaining the observed patterns of regional sea-level variability.

The model has some skill at reproducing the tide gauge records as shown by a comparison of the observed (black) and modeled (red) MSL values in Figure 2. Zero-lag correlations between the two sets of MSL are typically ~0.6 (Figure 6), apart from the most northern stations where the amplitude of the coastal variability is less. Correlations for stations south of Cape Hatteras are similar to those in the north. Gaps in the hydrographic sampling of the ocean, particularly as on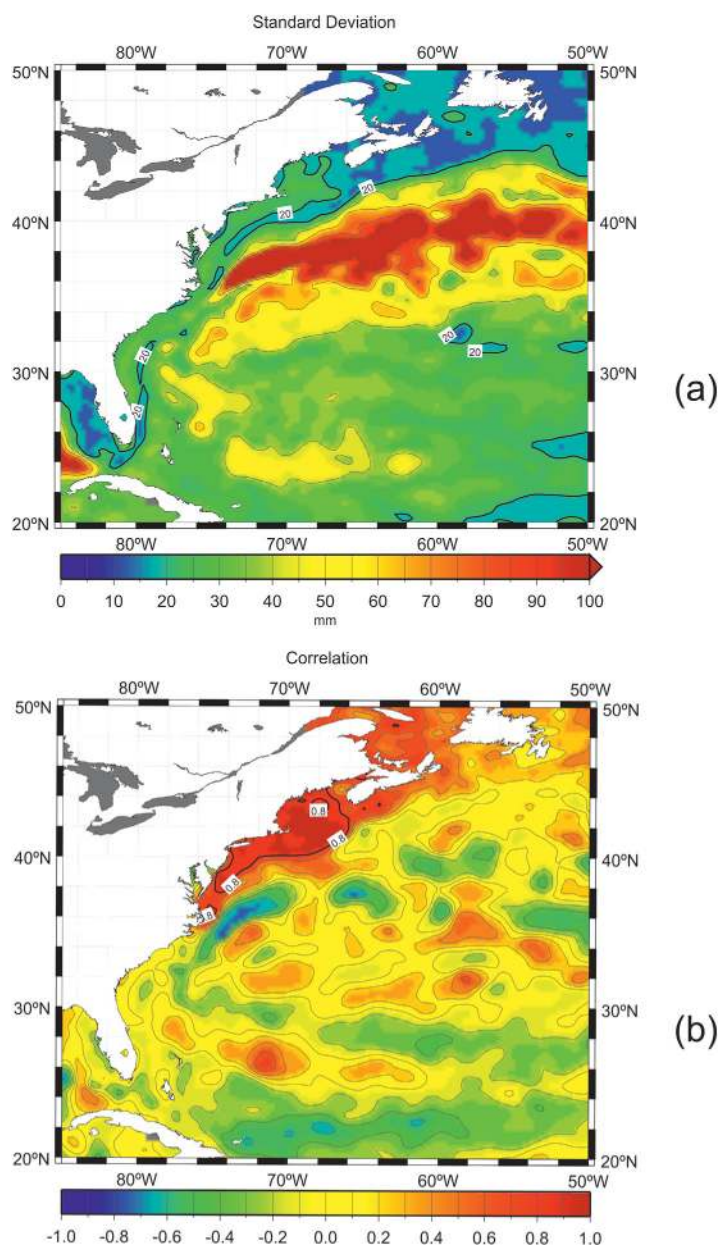e goes back in time, could have resulted in lower correlations than might otherwise have been obtained. Mismatches between measured and modeled MSL are similar in each section of coastline, suggesting either a common source of MSL variability that is not represented in the model, or an inadequacy in the model forcing and/or formulation. Two periods of mismatch that can be seen in Figure 2 include the early 1970s, which have importance to the discussion of accelerations in MSL below, and during the late 1990s. The former mismatch occurs for south of Cape Hatteras stations as well as for those to the north. Zervas [2009] noted that there had been anomalously high sea levels in the late 1990s from Providence to Wilmington in the MAB, and remarked that they occurred around the 1997–1998 El Niño (although the reasons for any relationship with El Niño were not discussed). There are similar mismatches to some extent at GOM and AC stations, but not for those to the south of Cape Hatteras. However, the period of mismatch is longer than the El Niño period, so its source remains unclear.

3.3. The Dynamical Assimilation and Use of Wind Information in the LHC Model

In order to obtain plausible sea-level reconstructions, the model investigations make use of a scheme that includes a repeated assimilation of annual temperature and salinity data, rather than a free model that suffers from long-term drift. For each year 1950–2009, the model is initialized in January with the annual UK Met Office/Hadley Centre temperature and salinity fields for the year, and integrated for 13 months to allow dynamically adjusted velocity and density fields to form; drift is minimized by including a weak 3-D relaxation to the initial fields with a 3 year time constant. The resulting density data contain gyre-scale undulations of the pycnocline and west-east boundary contrasts in density, which via thermal-wind balance induce corresponding horizontal gyre circulations and meridional overturning circulations; for further details see *Williams et al.* [2014] and *Lozier et al.* [2010]. For example, the meridional overturning circulation reaches 17.5 Sv (1 Sv = 10^6 m^3/s) between 40 and 50°N and there is decadal variability in the overturning transport of up to ± 2 Sv, often with opposing signals in the subtropical and subpolar gyres. Over shelf areas, the hydrographic fields are extrapolated from those in the neighboring deep ocean. In order to generate surface Ekman circulations, the NCEP monthly mean wind stresses are included, with month 13 stresses copied from those of month 1, thereby providing annual mean wind stresses for computation of calendar annual MSLs by averaging months 2–13.

Figure 4. (a) Standard deviation of detrended annual mean values of sea surface height from altimetry over the period 1993–2009. (b) Correlations of detrended annual mean values with those at a point on the shelf to the east of Cape Cod (42°N, 69°W).

The model can be expected to represent well the thermohaline circulation (including the thermohaline component of the MOC), as that is determined by assimilating the hydrography at the start of each year. The long-term effect of wind is included indirectly as the winds play a major role in establishing those hydrographic conditions. Over the shelves and near the coast, the imposed wind stress will also be a direct driver of shallow-water processes that can be fully established in the year, such as those discussed in section 5.

The model will not represent well the mesoscale variability located along the path of the Gulf Stream (Figure 4a). This deficiency arises primarily because the repeated model initialization from the hydrographic data prevents an independent eddy field developing from baroclinic instabilities. At Bermuda, south of the energetic mesoscale band, the model describes interannual sea level variability well, with a correlation coefficient of 0.71 between measured and modeled MSL during 1950–2009 (supporting information Figure S2). In addition, the model simulates adequately the linear trend in MSL in the North Atlantic observed by altimetry in the last two decades (supporting information Figure S3)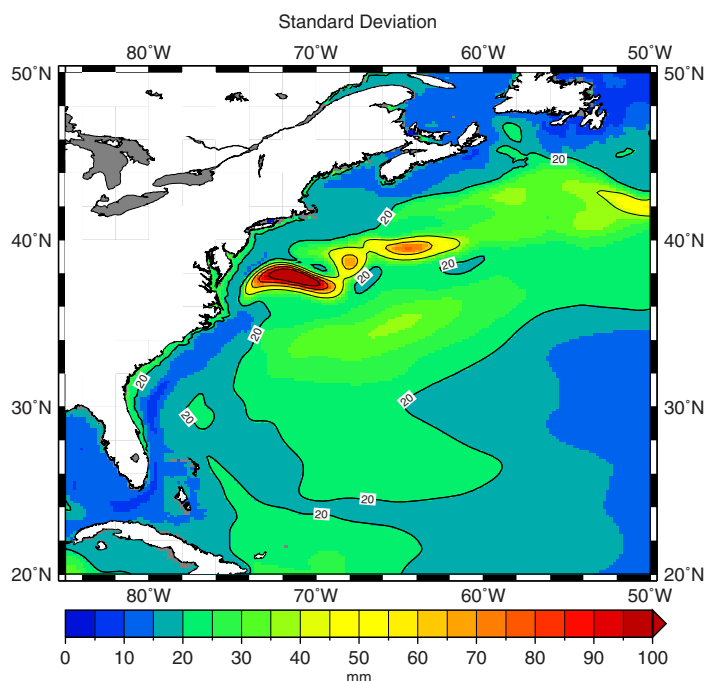. The differences between the model runs with and without wind forcing described below demonstrate what might be called the "direct" effects of the wind on the sea level and circulation, while the role of the wind in establishing the large-scale circulation is implicit in the hydrography.

3.4. Model Findings on the Role of the Wind
The coastal MSL variability in the model (Figure 5 and supporting information Figure S1) has been confirmed as being primarily due to the direct wind stress forcing by running a 1-degree version of the model for the same period, with and without wind forcing. Figures 7a and 7b show that standard deviations in the two cases, confirming that the coastal variability is not present without the wind forcing. In addition, as might have been anticipated, the wind plays a role in exciting more variability in the Gulf Stream gyre in Figure 7a. The coastal variability remains in a model run with wind forcing and with ocean temperatures

Figure 5. Standard deviation of detrended annual mean values of sea level from the higher resolution version of the LHC model over the period 1993–2009.

and salinities set to their climatological means throughout the run, although with reduced amplitude, while a further run with ocean forcing, but with climatological mean winds used each year, produces no coastal variability, similar to the run without wind forcing (not shown). Altogether these model runs demonstrate the important role of nearshore winds in generating the coastal sea-level variability (the slow propagation of baroclinic Rossby waves ensures that open ocean wind stress changes will predominantly influence coast sea level indirectly, via long-term hydrographic changes).

The importance of direct wind forcing is also clear by comparison to the tide gauge records.

Figure 2 shows that the 1 degree model with wind (blue) represents the tide gauge time series almost as well as the higher resolution model (red), while the model run without wind forcing (green) results in a poorer simulation of the measured MSL, albeit with a similar low-frequency component at the cm level. Figure 6 shows that the correlation between observed and modeled annual MSL is almost as good for the 1 degree model as for the higher resolution model, while the 1 degree model without wind forcing gives much smaller correlation coefficients.

Figure 6 provides a contrasting situation for stations south of Cape Hatteras (to the left of the dashed line), where correlations with all versions of the model are equally good, suggesting less of a "direct" effect of the wind in that area.

Insight into the spatial scales of interannual sea-level variability in the LHC model can be seen in Figure 8. In this example, Figure 8a plots correlations of variability with a test station (the model point closest to the Sandy Hook gauge in this case), showing once again the coherence of variability across the shelf, as in Figure 4b for altimetry. However, even though the variability is coherent, its magnitude is much reduced as one moves away from the coast. Linear regression, with annual sea levels at each model point and at Sandy Hook being the dependent and independent variables, respectively, gives the values of regression coefficient or "gain" shown in Figure 8b.

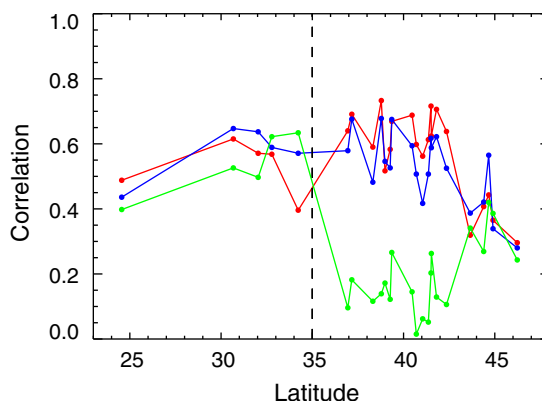The same conclusions are obtained using the 1 degree

Figure 6. Zero-lag correlation coefficients between detrended annual mean sea levels from the LHC model (higher resolution version, red; 1 degree version, blue; 1 degree version without wind forcing, green) and tide gauge MSL over the period 1950–2009. Measured MSL values were adjusted for the inverse barometer effect and the equilibrium lunar nodal tide. The dashed line at 35°N indicates Cape Hatteras.
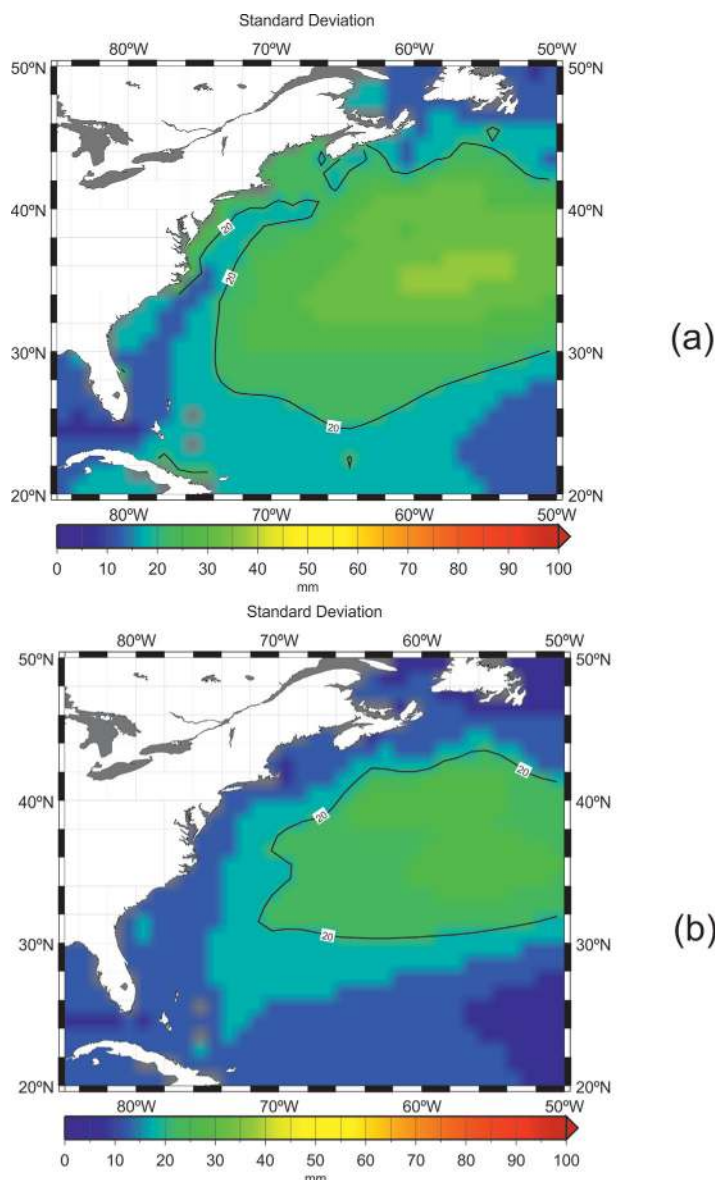
Figure 7. Standard deviations of detrended annual mean values of sea level from runs of the 1 degree version of the LHC model over the period 1950–2009 (a) with and (b) without wind forcing.

version of the model with wind forcing (Figures 9a and 9b), although the areas of high correlation and gain are larger than in Figures 8a and 8b. However, modified patterns are found without wind forcing (Figure 9c and 9d), higher correlations and gains extending across large parts of the shelf and even into the adjacent deeper NW Atlantic. Altogether, we conclude that the wind contributes to a sea-level variability that has maximum amplitude close to the coast, with coherent, lower amplitude variability as one moves out to the shelf edge; that these contributions are essential for describing a large part of the tide gauge record; and that these contributions from the wind add to a component that is more spatially coherent, and more uniform in amplitude, due to internal variability in the deep ocean.

3.5. MSL Variability With Several Years' Smoothing

MSL variability on longer timescales will result from the integrated effects of changes in water mass formation, including those due to MOC variability discussed in section 3.6, rather than the direct, wind-forced variability which has no oceanic memory from

year to year. Consequently, it is instructive to consider the MSL records of Figure 2 with mild smoothing.

Thompson and Mitchum [2014] undertook such a study of mildly low-passed MSL values, using a filter preserving timescales of variability approximately 2 years and longer, for the entire North American Atlantic coastline, Gulf of Mexico coast, and Caribbean Sea. Their focus was on coherent variability across the region that accounts for half of the total variance of the individual tide gauge records (see subsection 3.7 below).

However, there are major differences in MSL variability between subregions, as can be seen, for example, from inspection of their Figure 2, and from the present Figures 2 and 3. The standard deviations of coastline-average MSL records, constructed from the individual records in the MAB, GOM, and AC coastlines in Figure 2, are 19, 15, and 14 mm, respectively, for observed values, using a 3 year low-pass, box-car filter (comparable to the smoothing of *Thompson and Mitchum* [2014]). Those for the higher resolution model are 19, 14, and 8 mm, for the 1 degree model with wind forcing they are 16, 13, and 8 mm, and without wind forcing they are 9, 9, and 9 mm, respectively. In the Middle Atlantic Bight, the higher resolution and 1 degree models can
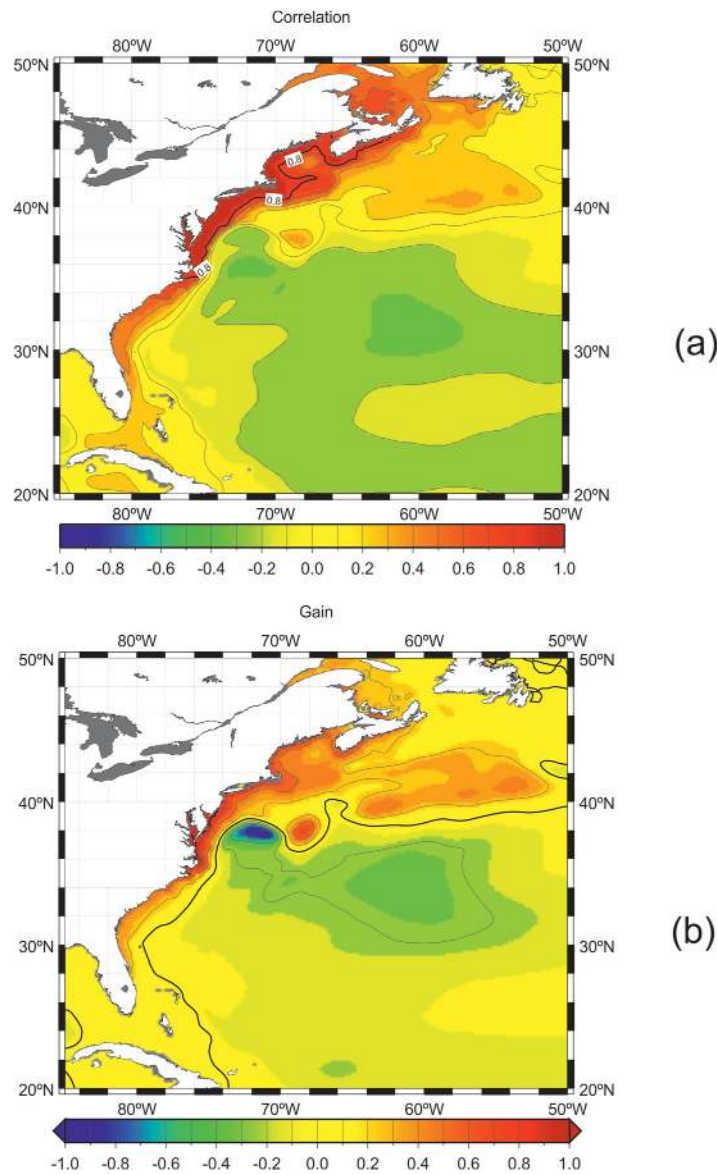
Figure 8. (a) Correlation coefficients of detrended annual mean values in the LHC model over the period 1950–2009 with those at a point near to Sandy Hook (74°W, 40.5°N). Contours are every 0.2. (b) Gains in sea level at each point in the model ocean with respect to sea level at Sandy Hook. Contours are shown every 0.25.

be seen to provide much of the interannual signal, with major negative years in the late-1970s and early 1980s. On the other hand, the model without wind forcing simulates a low-frequency component at the centimetre level that is also seen for the other models and for other coastlines. A similar situation pertains for the Gulf of Maine. In Atlantic Canada, all three models have similar low-amplitude behavior. The low-frequency component without wind forcing retains similar amplitude if smoothing is extended to 5 years.

3.6. Model Findings on the Role of the MOC

Bingham and Hughes [2009] proposed, based on considerations of geostrophy, that a 2 cm fall in MSL should result along this coastline if the overturning circulation strengthened by 1 Sv. This conclusion was suggested by a simple kinematic argument, and supported using a 1/4° version of the Ocean Circulation and Climate Advanced Modelling Project (OCCAM) ocean model for the short period 1985–2003. However, recent investigations of this model have led us to believe that local wind-related signals linked to a baroclinic response on the shelf may be missing in this particular model run.

Consequently, we have computed the Atlantic overturning transport at each latitude using the 1 degree LHC model for the extended period 1950–2009, with transport calculated between 100–1300 m depth and omitting surface waters so as to exclude surface Ekman transports. Figure 10 suggests that the overturning transport anomaly varies between ± 1 Sv, with reversals in the early 1970s and mid-1990s, slightly earlier in each case at higher latitudes. These time series are more low-frequency in character than the MSL records of Figure 2. The latter part of the time series at 50°N is similar to that computed by *Bingham and Hughes* [2009] using OCCAM (their Figure 2). The similarity of the black and blue curves in Figure 10 demonstrates that the wind plays only a minor direct role in determining the subsurface (100–1300 m) overturning transport.

Figure 11a shows correlation coefficients between model sea level and overturning transport at the same latitude, with transport again calculated between 100 and 1300 m depth. While there is negative correlation on the American seaboard south of Cape Hatteras and north of Newfoundland, there is only a weak
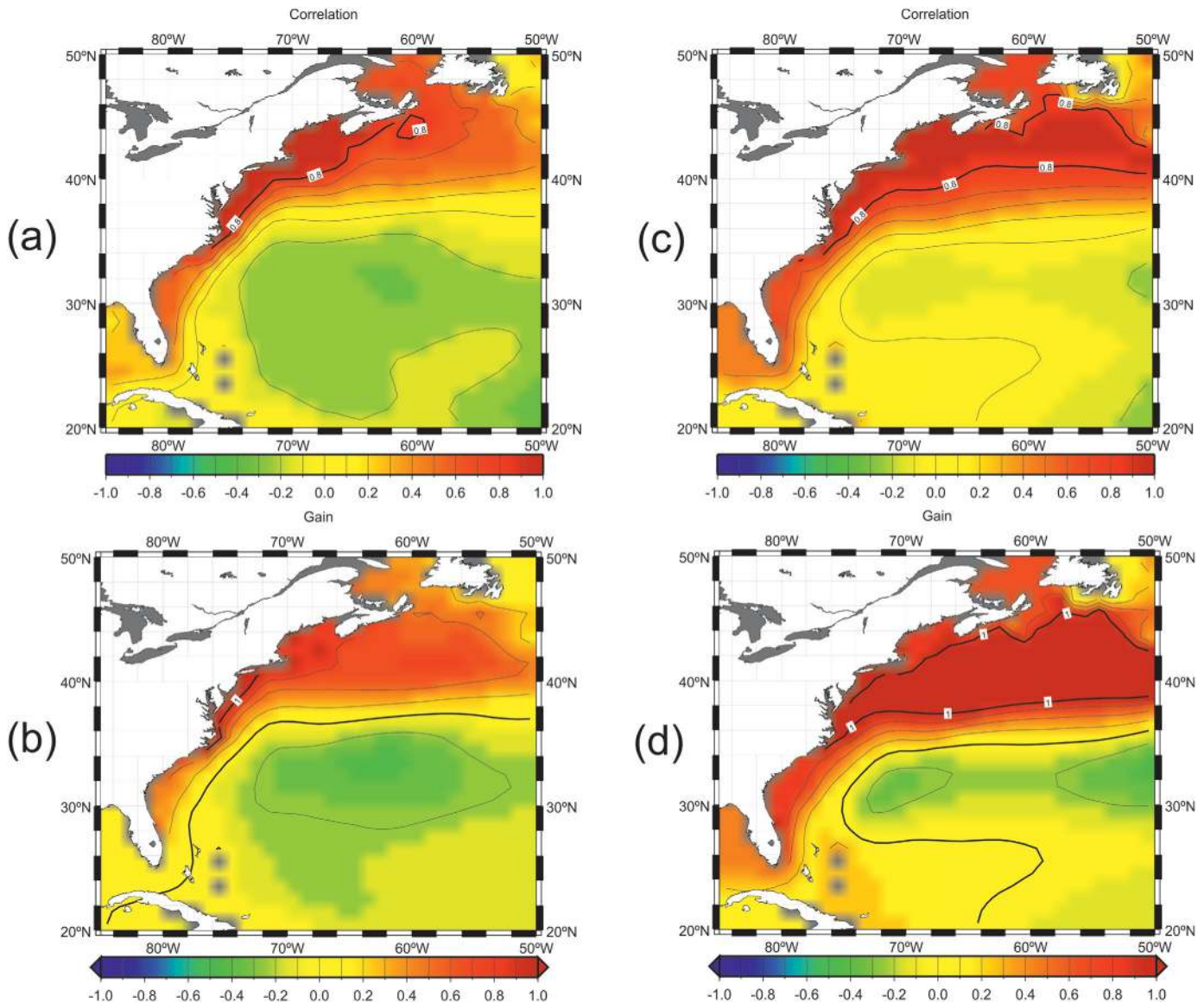
Figure 9. (a) Correlation coefficients of detrended annual mean values in the 1 degree version of the LHC model over the period 1950–2009 with those at a point near to Sandy Hook. Contours are every 0.2 between ±1. (b) Gains in sea level at each point in the model ocean with respect to sea level at Sandy Hook. Contours are shown every 0.25. Figures 9c and 9d are as for Figures 9a and 9b but without wind forcing.

negative correlation between Cape Hatteras and Newfoundland, implying that the changes in sea level along that coastline have not been controlled by changes in the strength of the overturning circulation in this period. Similar conclusions are obtained using transports computed for 0–1300 m depth. Furthermore, although it is reasonable to expect that MOC-related sea level changes might become a larger contributor to the total at longer timescales, similar findings are obtained with the yearly time series smoothed with windows of up to 11 years.

Figure 11b presents the corresponding map from the 1 degree model without wind forcing. Correlations along the entire length of the shelf are seen to be much more strongly negative, demonstrating a clear association between coastal sea level and overturning transport, qualitatively consistent with the conclusions of *Bingham and Hughes* [2009] using a model that (as mentioned above) seems to have had an inadequate representation of wind-driven baroclinic variability over the shelf. An increase in overturning transport of 1 Sv is found to correspond to a fall in coastal sea level of typically ∼1.5 cm (Figure 11c), a little lower than the value obtained by *Bingham and Hughes* [2009], probably due to the coarser model resolution in the present case.
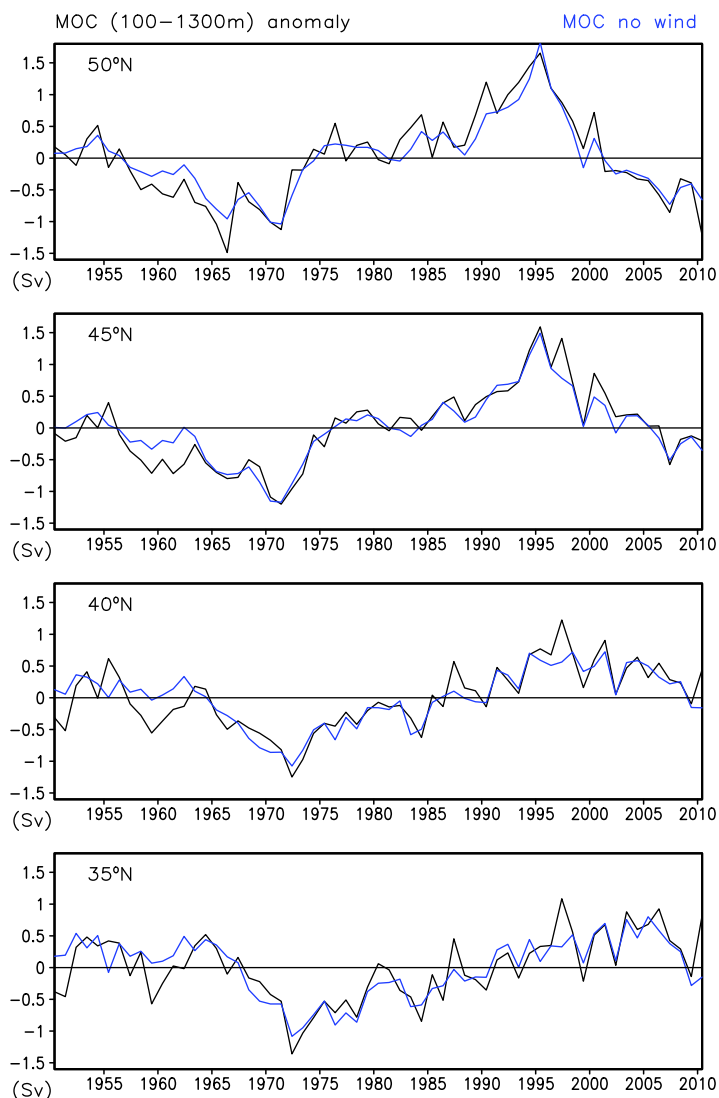
Figure 10. Annual mean values of the subsurface (100–1300 m) overturning transport anomaly from 34 to 50°N (black lines) using the 1 degree version of the LHC model. Blue lines indicate transports from a run with no direct wind forcing, indicating that transports are determined almost exclusively from the assimilated hydrographic fields.

Figure 11 suggests that, while there may indeed be a small component of coastal sea level variability related to the overturning circulation, any overall observed variability will be dominated by the wind forcing on the timescales under study, resulting in the weak correlations north of Cape Hatteras of Figure 11a.

We have repeated this analysis focussing on the periods 1985–2003, as used by *Bingham and Hughes* [2009], and 1950–2000, which corresponds to the period of generally increasing overturning transport in Figure 10, with the same conclusions as to the dominance of wind forcing over overturning transport in determining the variability of coastal sea level. The available model run does not allow the possible contribution of lower frequency MOC changes to MSL variability to be investigated (e.g., 60 year timescale, *Chambers et al.* [2012]).

One concern has been whether there is any impact on MOC conclusions of using a volume-conserving Boussinesq model, rather than a mass conserving non-Boussinesq model. However, we expect there to be differences in the mean fields using the two modeling approaches of only a few percent as demonstrated both theoretically and numerically [e.g., *Greatbatch et al.*, 2001; *Losch et al.*, 2004].

Although the MOC appears to be only weakly associated with MSL variability on interannual-decadal timescales, it has importance to other ocean parameters. For example, MOC variability at all latitudes is correlated negatively with western deep ocean heat content on typically 5 year timescales (R.G. Williams, et al., Impact of gyre-specific overturning changes on North Atlantic heat content, submitted to *Journal of Climate*, 2014), and the MOC often has opposing gyre signals on decadal timescales [*Lozier et al.*, 2010]. Other dynamical forcings may be as important for sea level, such as locally or remotely generated buoyancy and steric changes or remotely driven gyre dynamics (e.g., *Andres et al.* [2013] showed that MSL anomalies along the northeastern American coast are correlated significantly with wind stress curl in the subpolar gyre).

3.7. Northwest Atlantic Common Mode
The observations of *Thompson* [1986], that there are different régimes of MSL variability north and south of Cape Hatteras, were based on relatively short (25 year) records and will have been appropriate more for
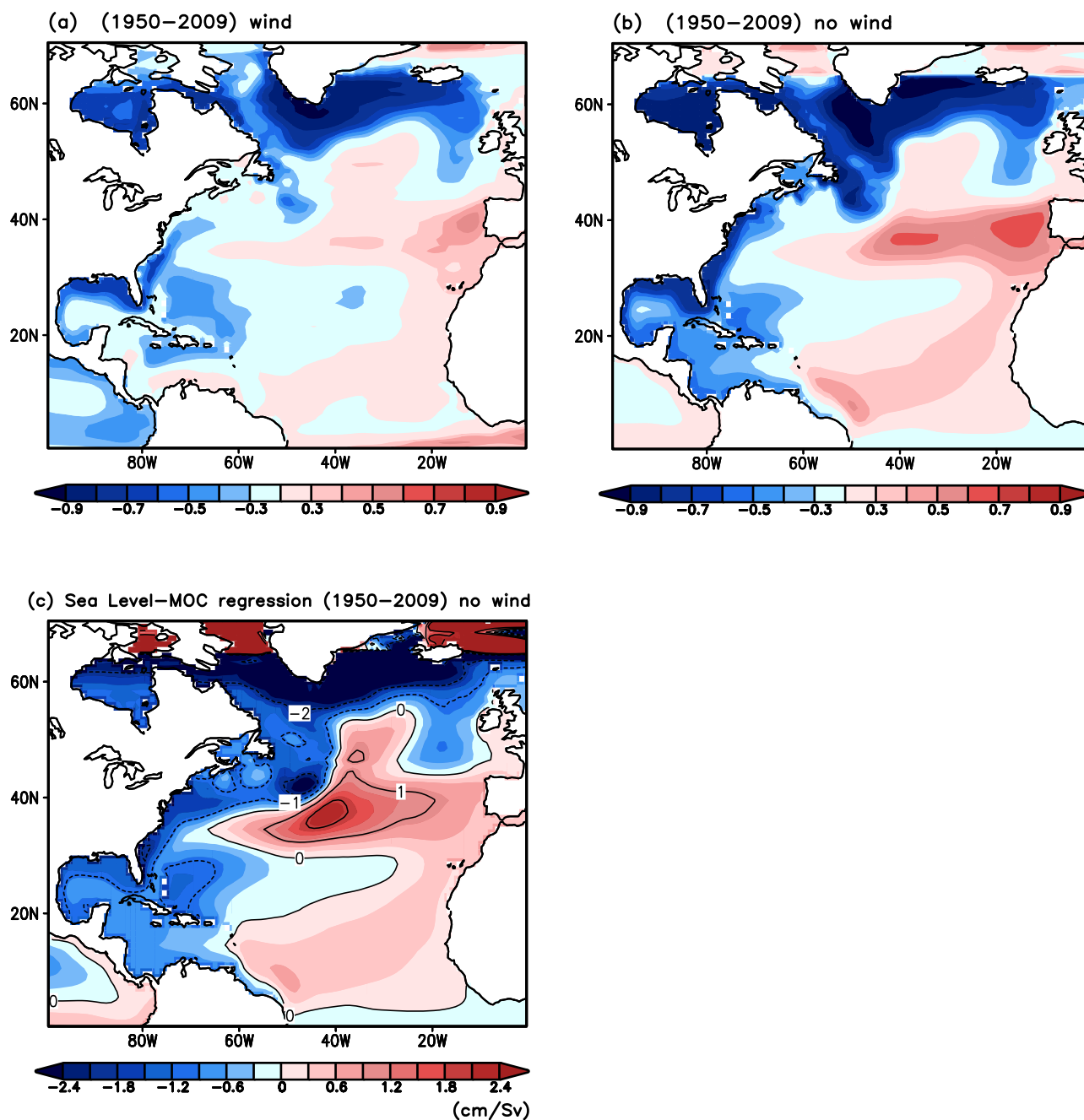
Figure 11. (a) Correlations of detrended values of annual mean sea level and overturning transport at the same latitude for depths between 100 and 1300 m using the 1 degree version of the LHC model for the period 1950–2009. (b,c) Corresponding correlations and regression coefficients (overturning transport as the independent variable) using the 1 degree model without wind forcing.

study of interannual than decadal variations. *Häkkinen* [2000] later pointed out that at decadal timescales the variations at stations either side of the Cape are, in fact, coherent.

The existence of spatially-coherent low-pass filtered MSL variability (or a "common mode") along all North American Atlantic coastlines has recently been demonstrated by *Thompson and Mitchum* [2014]. We shall not discuss that further here, except to remark that the LHC model without wind forcing simulates a similar "common mode." Figure 12 shows time series of MSL that are averages of model values at the tide gauge positions in Table 1. Similar ranges of variability (approximately ± 20 mm) are found for each section of coast, north and south of Cape Hatteras, and for the average for the whole northwest basin (80–65°W, 20–
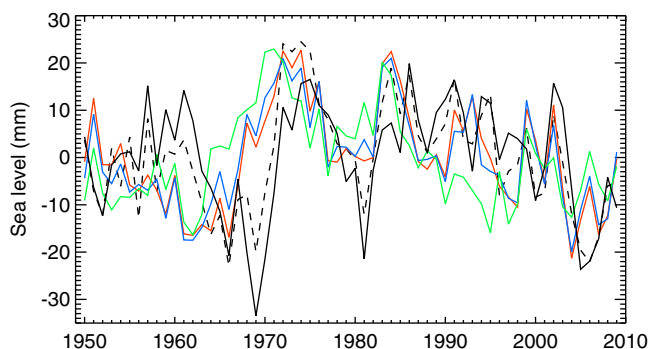
Figure 12. Average time series of MSL from the 1 degree version of the LHC model without wind forcing at Middle Atlantic Bight (red), Gulf of Maine (blue), Atlantic Canada (green), and South of Hatteras (black-dashed) stations. The solid black line shows basin average MSL from the model using cosine latitude weighting of the square grid for the northwest basin 80–65°W and 20–50°N.

50°N). The latter is almost identical to the basin average time series of *Thompson and Mitchum* [2014] computed from the German Estimating the Circulation and Climate of the Ocean (GECCO) model (their Figure 11), as is the difference between the curves for north and south of Cape Hatteras (their Figure 5). The basin average curve is strongly correlated at zero-lag with that for south of Cape Hatteras, with a coefficient of 0.82. Correlations for the sections of coast to the north are weaker (0.28, 0.13, and −0.23 for MAB, GOM, and AC, respectively), which can be seen to be primarily due to the lags in the large signals around 1970.

An overall conclusion from their and our models in combination is difficult to make, insofar as they diagnose the common mode in terms of divergence of Sverdrup transport, from wind stress curl fields, whereas in this particular LHC model run there is no explicit wind forcing at all, any wind-related effects being indirectly reflected in the hydrographic conditions for each year which have been specified by the Met Office fields. Nevertheless, whatever its source, a "common mode" of some kind does seem to exist at the centimetre level.

3.8. MSL Variability in Other Ocean Models
We have made investigations of MSL variability in this region using other ocean models. These are listed in supporting information and a summary of findings given. Our conclusion is that the LHC model is better at simulating the interannual variability in MSL observed by tide gauges and altimetry, than most of the other models (apart from the NEMO 1/4° model). None of the models are complete. For example, they do not include the changes in ocean mass which are known to have taken place during the second half of the 20th century due to exchanges between the ocean and cryosphere and terrestrial hydrosphere [*Church et al.*, 2014]. Also they do not consider river runoff that is thought to play a small role in observed MSL variability [*Meade and Emery*, 1971]. In addition, the input to the shelf circulation from the Labrador Current may not be represented adequately if Arctic processes are not included in the model.

4. Observed and Modeled Long-Term Accelerations in MSL

Close inspection of Figure 2 shows that many records from the region possess what appears to be a quadratic time-dependence (acceleration) since the mid-20th century. Acceleration over the shorter period 1969–2009 was even larger, thanks to the few years of high MSL at the start of the 1970s, especially for MAB stations. The regional character of the signal led to the suggestion of an MOC fingerprint [*Boon*, 2012; *Sallenger et al.*, 2012]. However, levels have declined once again since 2010 at many stations, as can be seen from the latest data on the PSMSL web site.

Accelerations are measured by means of a quadratic fit to the data:

$$MSL = a + bt + ct^2$$

where t is time and a, b, and c are coefficients determined from the fit, the quadratic coefficient "c" being half of the acceleration. Figures 13a and 13b provide values of "c" for the two periods of interest, 1950–2009 and 1969–2009, respectively, demonstrating that coefficients differ north and south of Cape Hatteras in both periods. The coefficients are largely unaffected by applying the inverse barometer correction or not. (Figure 13 also shows the average standard errors for each set of coefficients calculated from annual values. Consideration of serial correlation would increase the standard errors. However, note that we are not
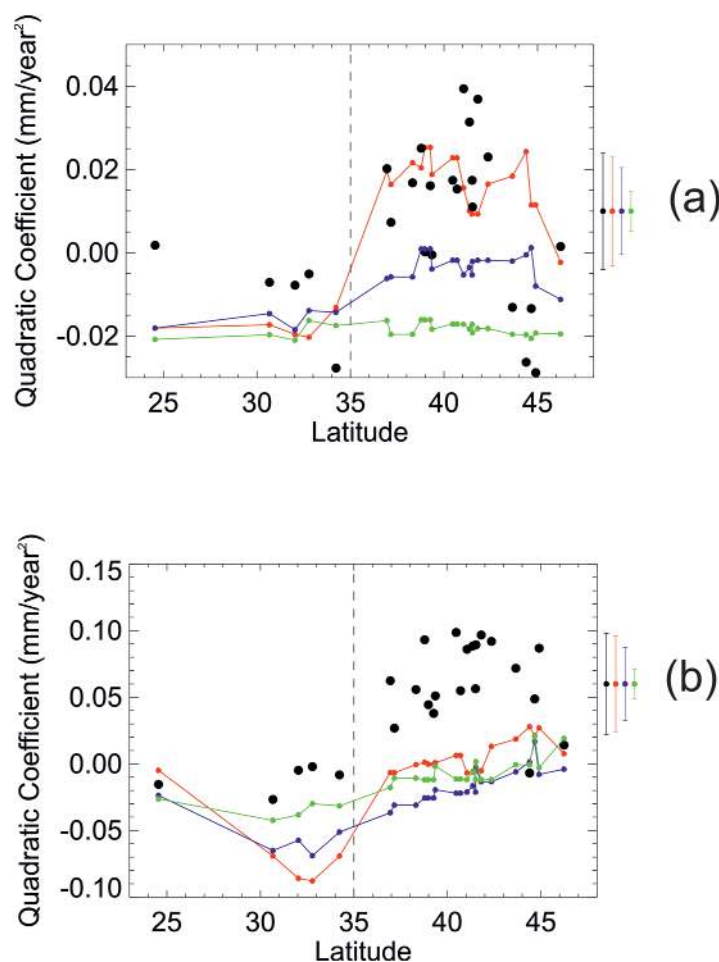
Figure 13. Quadratic coefficients obtained from regression fits to tide gauge MSL records for the periods (a) 1950–2009 and (b) 1969–2009 (black dots). MSL values have been adjusted for the inverse barometer effect. Red, blue, and green dots refer to quadratic coefficients in the higher resolution LHC model, 1 degree version, and 1 degree version without wind forcing, respectively. The error bars on the right show the average standard errors for each set of coefficients calculated using annual values. The dashed line at 35°N indicates Cape Hatteras.

claiming statistical significance for any quadratic coefficients here. Rather, we are testing how coefficients vary spatially, and investigating the origins of accelerations which have received attention in the literature.)

The higher resolution version of the LHC model provides similar quadratic coefficients to the tide gauges for 1950–2009 (red and black dots, respectively, in Figure 13a). The model shows that coefficients are most positive just to the north of Cape Hatteras, reducing slightly travelling north (although several northern stations in the Gulf of Maine and Atlantic Canada disagree with that trend in having more negative values for measured than modelled MSL). Coefficients are smaller or even negative (in measured MSL) and negative (in the model) south of Cape Hatteras, indicating again the differences between sections of coastline. The coefficients for the 1 degree version (blue dots) are smaller than for the higher resolution version north of Cape Hatteras, probably due to the limitations of resolving the dynamics in a narrow coastal strip (Figure 14 below). However, they are similar to the higher resolution values in that, with their wind forcing, they are again more positive than those to the south of Cape Hatteras. Without wind forcing in the 1 degree version (green dots), the quadratic coefficients are similarly negative both north and south of the Cape.

Figure 14 provides a map of quadratic coefficients from the higher resolution version of the model. The general agreement at the tide gauges (Figure 13) can be seen to be due to a narrow band of positive coefficients, similar to the coastal band of high variability in Figure 5 and supporting information Figure S1, emphasizing the important contributions from the wind to MSL variability near the coast.

Figure 15 shows a map of "acceleration vectors" of NCEP wind stresses for 1950–2009. This map represents the 2-dimensional values of "c" for wind stress in units of 10^{-4} N/m^2/yr^2. It shows that wind stress accelerated over the Scotian Shelf in an almost exactly westward direction, with smaller westward values to the south as far as Cape Hatteras. This pattern, roughly along-shore along the Scotian Shelf and Gulf of Maine and almost on-shore further south, is similar to that found by *Thompson* [1986] for the response of coastal MSL to local wind stress. One can also use the estimated "rule-of-thumb" of *Andres et al.* [2013], that the typically ± 50 mm variability in annual MSL is due to (0.04–0.1) 10^{-4} N/m^2 variability in along-shore wind stress along the Scotian Shelf and Gulf of Maine (see section 5 below). Therefore, the ~0.1 10^{-4} N/m^2/yr^2 seen for the quadratic coefficients in wind stress in this region at approximately 43° N and between 69.4
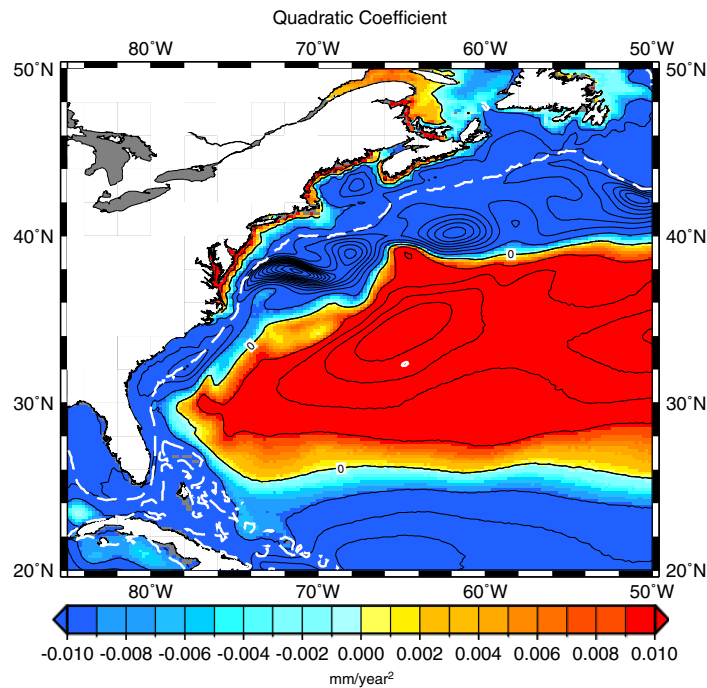
WOODWORTH ET AL.   14

Figure 14. Quadratic coefficients obtained from regression fits to sea levels from the LHC model for the period 1950–2009. The dashed line indicates the 500 m isobath. Contours are every 0.01 mm/yr^2.

and 61.8°E in Figure 15 would correspond to quadratic coefficients ("c") for sea level of ~0.01 mm/yr^2, of a similar order of magnitude to the observed values. (The NCEP wind stress product has an approximately 2° grid and this geographical selection averages over five grid points.) Figure 15 confirms that the wind played a part in the MSL acceleration in this period, as can also be inferred by comparing the red and green curves, for MAB and GOM especially, in Figure 2, and as demonstrated by Figure 13a. (See also *Calafat and Chambers* [2013] who were able to account for acceleration in MSL at stations in this area for approximately the same period using regressions with meteorological and climate indices.)
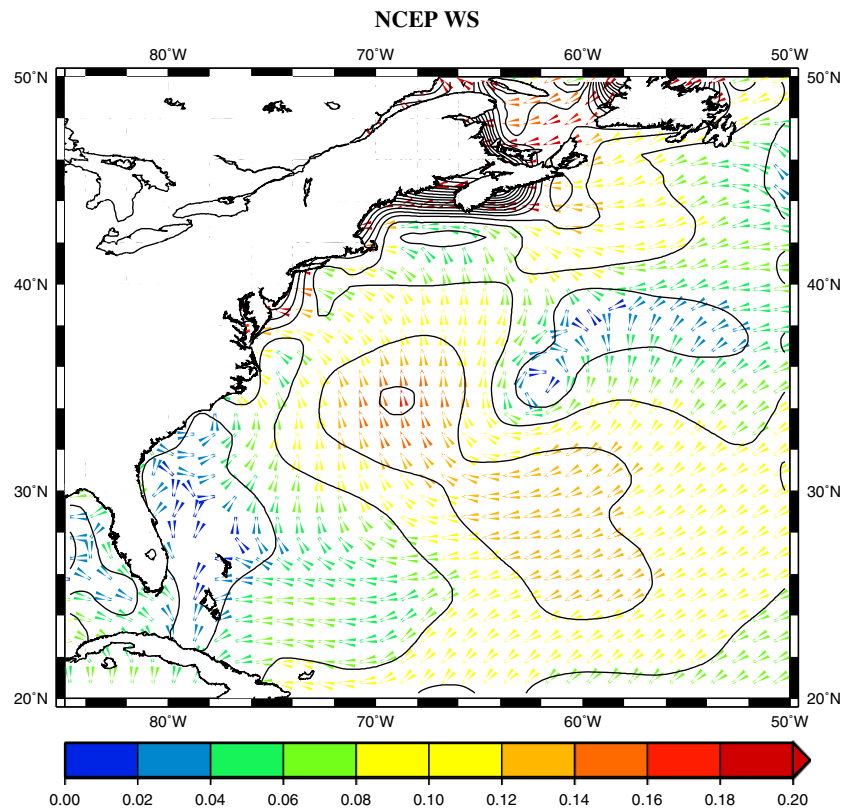

Figure 15. Quadratic coefficients obtained from regression fits to NCEP annual wind stress over the period 1950–2009. Units are 10^{-4} N/m^2/yr^2.

The model does not explain the large acceleration in recent years during 1969–2009 (or 1969–2011 in the *Boon* [2012] analysis). In this period, the quadratic coefficients obtained from the tide gauges are considerably larger than in the model (Figure 13b), although the difference appears to be caused by a mismatch between model and tide gauge MSL of just a few centimetres in the early 1970s, near the start of this short recent period (Figure 2). (This underlines that the estimation of quadratic coefficients from short spans of either measured or modeled MSL is highly imprecise, with real uncertainties in quadratic coefficients undoubtedly larger than the formal ones, and that accurate estimates of acceleration can be obtained only over longer periods.) The model does, however, once again demonstrate an increase of coefficients with latitude, in particular for either side of Cape Hatteras, consistent with the observations. That is why *Sallenger et al.* [2012] referred to the MAB as a "hot spot," rather than the coast to the south of the Cape.

We investigated this period further with regard to the role of the overturning circulation, as its possible importance in this period had already been suggested by other authors [e.g., *Sallenger et al.*, 2012; *Ezer et al.*, 2013]. At first sight, the overturning transport time series in the north of the region displays an interesting change of character during the mid-1990s, with transports declining throughout the 2000s (Figure 10). The timing of this reversal corresponds roughly to the midpoint of the reported recent acceleration of sea level in the Middle Atlantic Bight and Gulf of Maine. However, the 1 degree model shows no overall significant correlation north of Cape Hatteras between coastal sea level and MOC, for model runs either with or without wind forcing (i.e., there are much weaker patterns in this short period than for the whole model run shown in Figure 11c). Therefore, the LHC model cannot support an MOC explanation for this short-term acceleration.

Our model runs do not allow us to consider the role of the MOC on MSL changes at the coast over longer timescales. However, it is possible to consider the possible role of wind stress in long-term MSL acceleration, thanks to the availability of the 20CR data set. At New York, a "*c*" value of 0.0038 mm/yr^2 was obtained using MSL data uncorrected for the inverse barometer for the period 1856–2009 (with a standard error of 0.0014 mm/yr^2, see *Woodworth et al.* [2011a]). This value is similar to those at NW European tide gauges [*Woodworth et al.*, 2011b], and compares qualitatively to information from northeast American and European salt marsh data [*Gehrels and Woodworth*, 2013; *Long et al.*, 2014]. The 20CR data set covers 1871–2012, comparable to the New York MSL record. It suggests a large-scale cyclonic pattern of acceleration vectors over the western North Atlantic (supporting information Figure S4). The vectors over the Scotian Shelf and Gulf of Maine are less zonal than in Figure 15. Nevertheless, if one scales the zonal quadratic coefficients at 43° N using the *Andres et al.* [2013] rule-of-thumb, then one infers a quadratic coefficient for sea level of approximately 0.0016 mm/yr^2. It is plausible, therefore, that acceleration in wind stress over the shelf could have played a part in the observed 19th–20th century acceleration in sea level along the North American coast. However, it is unlikely to provide a complete explanation and detailed numerical modeling over this extended period would be necessary to investigate this possibility further.

5. Discussion of Winds and Coastal MSL Variability in Idealized Models

We have shown that there is a spatially coherent signal of MSL variability along the North American Atlantic coast, and we have discussed, in the context of the LHC model, two different processes that are often invoked to explain the variability. These processes concern the role of nearshore winds on the shelf, and the larger-scale signal of changes in the meridional overturning circulation.

In this section, we consider the role of winds in terms of idealized dynamical balances and the possible link to the coastal variability evident in Figures 5 and 14. MSL variability along the Scotian Shelf has long been thought to be associated with variability in coastal flows and with along-shore wind stress. For example, *Thompson* [1986] investigated the simple analytic models of *Csanady* [1982] for along-shore wind stress τ^y acting on a wedge-shaped shelf:

$$\frac{\rho g \eta}{\tau^y} = \frac{fL}{r}$$

where ρ, g, and f are water density, acceleration due to gravity and Coriolis parameter respectively. For a realistic choice of bottom friction coefficient (r) of 5×10^{-4} m/s, he found that the cross-shelf scale of the wind-driven boundary current (L) must be only 10 s of km, given the observed magnitude of coastal sea-

level variability (η). Similarly, *Andres et al.* [2013], following *Sandstrom* [1980], considered the cross-stream geostrophic balance of a coastal flow that is zero at the shelf edge and largest at the coast, and along-shelf frictional balance for transport anomalies, and concluded that the ±50 mm of coastal sea level variability in the MAB, GOM, and AC must correspond to wind stress variability of approximately 0.04–0.1 N/m^2.

One can ask whether the observed spatial coherence of MSL might not be simply a reflection of coherence in the applied wind stress. Indeed, NCEP annual mean surface wind stresses over the shelves between Cape Hatteras and southern Nova Scotia have correlations with wind stress at Sandy Hook of 0.87 or higher i.e., Sandy Hook wind stress variability explains 75% or more of the annual mean wind stress variance in the whole area (supporting information Figure S5). This suggests that insight could be gained by considering the zonal response of sea levels over the shelf and slope to spatially uniform variability in the wind stress.

To investigate this, to first-order at least, we used a linear model similar to that of *Clark and Brink* [1985] to quantify the response of stratified, frictional flows to low-frequency oscillations in wind stress (see *Brink and Chapman* [1987] for model details, and *Huthnance* [2004] for its further development). The model uses linear equations appropriate for the description of a stratified Boussinesq fluid, solving for the velocity components (u, v, w), the perturbation density ρ (with respect to a background static stratification ρ_0), and the perturbation free surface η (with respect to $\eta_0 = 0$) in a longitude-depth domain with realistic bathymetry [*NGDC*, 1988] and (albeit horizontally uniform) background stratification [*NODC*, 1994]. Linear bottom friction uses a spatially uniform Rayleigh coefficient.

We used a model profile domain representing the meridionally averaged bathymetry of the GOM between 42 and 43.6°N. The profile spans 70–50°W from surface to seabed, encompassing both the shelf (approximately 650 km wide and 150 m deep on average) and the slope (which is over 4000 m deep at its eastern end). At the coast, the vertically integrated flow in the x direction is set to zero. At the $x = 50°$W boundary, the condition $u_x = 0$ is applied at all depths. The top and bottom boundary conditions are found by integration over the respective Ekman layers. The model is forced with a harmonic, along-shore wind stress spatially uniform in the offshore direction and of prescribed amplitude, frequency and wavelength in the along-shore direction. It then solves for the steady state amplitudes and phases of the harmonic velocity, buoyancy, and pressure (including free surface elevation) in response to the applied wind forcing. Since the problem is linear, the amplitude of the wind stress is fixed to 0.1 N/m^2, which is of the order of the observed interannual wind standard deviation in the region.

Using wind stresses with periods between 1 month and 10 years and wavelengths of between 100 km and 10,000 km, and Rayleigh friction values of between 2.5×10^{-4} m/s and 10×10^{-4} m/s, we obtained a maximum response in η of about 30 (10) mm at the coast for the lowest (highest) frictional coefficient. This response is always trapped on the shelf (cf. Figure 5), but the width of the boundary current strongly depends on the wind's wavelength, λ. For $\lambda = 100$ km, the boundary current is confined to within 25 km from the coast, while for $\lambda = 10,000$ km the boundary current extends to the shelf edge, but not further.

These results are consistent with those obtained by *Thompson* [1986], and explain partly why the wind results in coastal variability, resulting in a band of low MSL variability near to the shelf edge. In addition, there are known to be coastal flows that originate from the Labrador Current, passing along the Scotian Shelf, Gulf of Maine, and Middle Atlantic Bight and tending to follow the isobaths. These mean flows are only a few tenths m/s (and transports a few tenths Sv) and may reverse at times [*Lentz*, 2008; *Shearman and Lentz*, 2010]. In the Gulf of Maine, surface currents are known to have a contribution from coastal buoyancy driven flows resulting from the contrast between freshwater inputs from rivers and higher density water over the central Gulf [*Gangopadhyay et al.*, 2003], although the mean flows along the Scotian Shelf [*Han et al.*, 1997] and Middle Atlantic Bight [*Lentz*, 2008] are further from the coast. In general, fluid dynamics conspire to make the continental slope a relatively quiet zone. For example, shelf waves will tend to remain trapped on the shelf and decay dramatically across the slope [*Huthnance*, 2004]. Meanwhile, deep ocean motions (both mean flows and variability) will encounter a barrier at the slope [*Smith*, 1983; *Loder et al.*, 1998]. Likewise, eddies, be they generated on the shelf or the deep ocean, will find it difficult to cross the slope, as that requires large changes in vorticity.

These simple arguments suggest that the MSL variability close to the coast shown by the LHC model is plausible, although given the model's 1/6° resolution it may not be resolved as well as possible. The LHC model is clearly not perfect, as shown by the correlation coefficients of Figure 7 being some distance from 1.0,

indicating that more work is required to understand the overall MSL variability. However, it does appear to simulate the variability on the shelf north of Cape Hatteras more realistically than some other models. It is worth noting that the presence of stratification is necessary for production of a response of reasonable amplitude. Much smaller amplitudes arise in barotropic models. The need for maintenance of appropriate stratification in the shelf region may explain why models with similar wind stresses are found to produce quite different coastal responses (see supporting information).

6. Conclusions

Observations of MSL variability from tide gauges and altimetry, and simulations of the variability using an ocean model, have provided new insight into its overall spatial and temporal scales in the northwest Atlantic and along the coasts of the US and Canada north of Cape Hatteras. The LHC model has demonstrated how nearshore wind forcing plays an important role on all timescales (interannual and longer) on different sections of coast, with the MSL variability associated with the wind largest near the coast and diminishing off-shore. Meanwhile, a model run without wind forcing has shown how smaller and lower frequency signals can occur in each section of coast due to large spatial-scale processes in the North Atlantic.

The study has suggested that the nearshore wind can contribute to variability over long timescales, with the LHC model simulation of a coastal acceleration in sea level over the model run (1950–2009) consistent with that in tide gauge MSL, although it fails to account adequately for the much-discussed larger acceleration in the Middle Atlantic Bight in the shorter recent period since the mid-1980s. As *Kopp* [2013] has stressed (see also *Ezer et al.* [2013] and *Rossby et al.* [2014]), much longer time series will be needed to properly assess the significance of that particular acceleration. At present, it seems that MSL along the northeast American coastline has stabilized or is falling again.

If the coastal variability suggested by the model is real, it is a reminder that MSL variability observed by tide gauges can result from many local and regional processes (and be sensitive to details of nearshore stratification), as well as from the basin- and global-scales ones that are usually the focus of climate studies. For example, recent papers have demonstrated the importance of along-shore winds on the eastern boundary of the North Atlantic in understanding NW European and Mediterranean MSL [*Sturges and Douglas*, 2011; *Calafat et al.*, 2012].

By contrast, the model has demonstrated that variability in the overturning circulation, which has been discussed extensively in the recent literature as a possible cause of MSL acceleration, appears to be less important than the directly wind-induced variability. The MOC correlates only weakly with sea level at the coast and on the shelf north of Cape Hatteras, at least for the interannual and decadal timescales sampled by our model runs. Although there is a clear negative correlation in a model run without wind forcing, with a decrease of 1 Sv in overturning transport corresponding to an increase of ~1.5 cm in sea level, consistent with previous studies [*Bingham and Hughes*, 2009], when wind forcing is applied it is found to dominate the overall variability and to destroy any such correlation. Coastal MSL in the model run without wind forcing appears better associated with a plausible centimetric "common mode" of spatially coherent MSL variability, as suggested by *Thompson and Mitchum* [2014] to be due to divergence of Sverdrup transport in the northwest Atlantic.

Longer model runs that employ 20CR meteorological fields, for example, may provide further insight into the relative importance of these different forcings of MSL variability and acceleration on different timescales.

References

Andres, M., G. G. Gawarkiewicz, and J. M. Toole (2013), Interannual sea level variability in the western North Atlantic: Regional forcing and remote response, *Geophys. Res. Lett.*, *40*, 5915–5919, doi:10.1002/2013GL058013.

Bingham, R. J., and C. W. Hughes (2009), Signature of the Atlantic meridional overturning circulation in sea level along the east coast of North America, *Geophys. Res. Lett.*, *36*, L02603, doi:10.1029/2008GL036215.

Boon, J. D. (2012), Evidence of sea level acceleration at U.S. and Canadian tide stations, Atlantic coast, North America, *J. Coastal Res.*, *28*, 1437–1445, doi:10.2112/JCOASTRES-D-12-00102.1.

Brink, K. H., and D. C. Chapman (1987), Programs for computing properties of coastal-trapped waves and wind-driven motions over the continental shelf and slope, *Tech. Rep. WHOI-87-24*, 199 + iii pp, Woods Hole Oceanogr. Inst., Mass.

Calafat, F. M., and D. P. Chambers (2013), Quantifying recent acceleration in sea level unrelated to internal climate variability, *Geophys. Res. Lett.*, *40*, 3661–3666, doi:10.1002/grl.50731.

Calafat, F. M., D. P. Chambers, and M. N. Tsimplis (2012), Mechanisms of decadal sea level variability in the eastern North Atlantic and the Mediterranean Sea, *J. Geophys. Res.*, *117*, C09022, doi:10.1029/2012JC008285.

Chambers, D. P., M. A. Merrifield, and R. S. Nerem (2012), Is there a 60-year oscillation in global mean sea level? *Geophys. Res. Lett.*, *39*, L18607, doi:10.1029/2012GL052885.

Church, J. A., et al. (2013), Sea level change, in *Climate Change 2013: The Physical Science Basis. Contribution of Working Group I to the Fifth Assessment Report of the Intergovernmental Panel on Climate Change*, edited by T. F. Stocker, et al., Chapter 13, pp. 1137–1216, Cambridge University Press, Cambridge, U. K.

Clarke, A. J., and K. H. Brink (1985), The response of stratified, frictional flow of shelf and slope waters to fluctuating large-scale, low-frequency wind forcing, *J. Phys. Oceanogr.*, *15*, 439–453, doi:10.1175/1520-0485(1985)015<0439:TROSFF>2.0.CO;2.

Compo, G. P., et al. (2011), The twentieth century reanalysis project, *Q. J. R. Meteorol. Soc.*, *137*, 1–28, doi:10.1002/qj.776.

Csanady, G. T. (1982), *Circulation in the coastal ocean*, 279 pp., D. Reidel, Dordrecht, Netherlands.

Department of Fisheries and Oceans (DFO), Canada (2014), Department of Fisheries and Oceans Canada Sea Level, Ottawa. [Available at tides.gc.ca.]

Ezer, T., L. P. Atkinson, W. B. Corlett, and J. L. Blanco (2013), Gulf Stream's induced sea level rise and variability along the U.S. mid-Atlantic coast, *J. Geophys. Res.*, *118*, 685–697, doi:10.1002/jgrc.20091.

Frankcombe, L. M., and H. A. Dijkstra (2009), Coherent multidecadal variability in North Atlantic sea level, *Geophys. Res. Lett.*, *36*, L15604, doi:10.1029/2009GL039455.

Gangopadhyay, A., A. R. Robinson, P. J. Haley, W. G. Leslie, C. J. Lozano, J. J. Bisagni, and Z. Yu (2003), Feature-oriented regional modeling and simulations in the Gulf of Maine and Georges Bank, *Cont. Shelf Res.*, *23*, 317–353, doi:10.1016/S0278-4343(02)00151-6.

Gehrels, W. R., and P. L. Woodworth (2013), When did modern rates of sea-level rise start?, *Global Planet. Change*, *100*, 263–277, doi:10.1016/j.gloplacha.2012.10.020.

Greatbatch, R. J., Y. Lu, and Y. Cai (2001), Relaxing the Boussinesq approximation in ocean circulation models, *J. Atmos. Ocean. Technol.*, *18*(11), 1911–1923, doi:10.1175/1520-0426(2001)018<1911:RTBAIO>2.0.CO;2.

Häkkinen, S. (2000), Decadal air-sea interaction in the North Atlantic based on observations and modeling results, *J. Clim.*, *13*(6), 1195–1219, doi:10.1175/1520-0442(2000)013<1195:DASIIT>2.0.CO;2.

Häkkinen, S. (2001), Variability in sea surface height: A qualitative measure for the meridional overturning in the North Atlantic, *J. Geophys. Res.*, *106*(C7), 13,837–13,848, doi:10.1029/1999JC000155.

Han, G., C. G. Hannah, J. W. Loder, and P. C. Smith (1997), Seasonal variation of the three-dimensional mean circulation over the Scotian Shelf, *J. Geophys. Res.*, *102*(C1), 1011–1025, doi:10.1029/96JC03285.

Holgate, S. J., A. Matthews, P. L. Woodworth, L. J. Rickards, M. E. Tamisiea, E. Bradshaw, P. R. Foden, K. M. Gordon, S. Jevrejeva, and J. Pugh (2012), New data systems and products at the Permanent Service for Mean Sea Level, *J. Coastal Res.*, *29*, 493–504, doi:10.2112/JCOASTRES-D-12-00175.1.

Hong, B. G., W. Sturges, and A. J. Clarke (2000), Sea level on the U.S. east coast: Decadal variability caused by open ocean wind-curl forcing, *J. Phys. Oceanogr.*, *30*, 2088–2098, doi:10.1175/1520-0485(2000)030<2088:SLOTUS>2.0.CO;2.

Huthnance, J. M. (2004), Ocean-to-shelf signal transmission: A parameter study, *J. Geophys. Res.*, *109*, C12029, doi:10.1029/2004JC002358.

Kalnay, E., et al. (1996), The NCEP/NCAR 40-year reanalysis project, *Bull. Am. Meteorol. Soc.*, *77*, 437–470, doi:10.1175/1520-0477(1996)077<0437:TNYRP>2.0.CO;2.

Kistler, R., et al. (2001), The NCEP-NCAR 50 year reanalysis: Monthly means CD-ROM and documentation, *Bull. Am. Meteorol. Soc.*, *82*, 247–267, doi:10.1175/1520-0477(2001)082<0247:TNNYRM>2.3.CO;2.

Kopp, R. E. (2013), Does the mid-Atlantic United States sea level acceleration hot spot reflect ocean dynamic variability?, *Geophys. Res. Lett.*, *40*, 3981–3985, doi:10.1002/grl.50781.

Lentz, S. J. (2008), Observations and a Model of the Mean Circulation over the Middle Atlantic Bight Continental Shelf, *J. Phys. Oceanogr.*, *38*, 1203–1221, doi:10.1175/2007JPO3768.1.

Levermann, A., A. Griesel, M. Hofmann, M. Montoya, and S. Rahmstorf (2005), Dynamic sea level changes following changes in the thermohaline circulation, *Clim. Dyn.*, *24*, 347–354, doi:10.1007/s00382-004-0505-y.

Loder, J. W., W. C. Boicourt, and J. H. Simpson (1998), Western ocean boundary shelves, in *The Sea, Volume 11: The Global Coastal Ocean: Regional Studies and Syntheses*, edited by A. R. Robinson and K. H. Brink, pp. 3–28, Wiley, N. Y.

Long, A. J., N. L. M. Barlow, W. R. Gehrels, M. H. Saher, P. L. Woodworth, R. G. Scaife, M. J. Brain, and N. Cahill (2014), Contrasting records of sea-level change in the eastern and western North Atlantic during the last 300 years, *Earth Planet. Sc. Lett.*, *338*, 110–122, doi:10.1016/j.epsl.2013.11.012.

Lorbacher, K., J. Dengg, C. W. Böning, and A. Biastoch (2010), Regional patterns of sea level change related to interannual variability and multidecadal trends in the Atlantic Meridional Overturning Circulation, *J. Clim.*, *23*, 4243–4254, doi:10.1175/2010JCLI3341.1.

Losch, M., A. Adcroft, and J.-M. Campin (2004), How sensitive are coarse general circulation models to fundamental approximations in the equations of motion?, *J. Phys. Oceanogr.*, *34*(1), 306–319, doi:10.1175/1520-0485(2004)034<0306:HSACGC>2.0.CO;2.

Lozier, M. S., V. Roussenov, M. S. C. Reed, and R. G. Williams (2010), Opposing decadal changes for the North Atlantic meridional overturning circulation, *Nat. Geosci.*, *3*, 728–734, doi: 10.1038/NGEO947.

Marshall, J., C. Hill, L. Perelman, and A. Adcroft (1997a), Hydrostatic, quasi-hydrostatic, and nonhydrostatic ocean modelling, *J. Geophys. Res.*, *102*(C3), 5733–5752, doi:10.1029/96JC02776.

Marshall, J., A. Adcroft, C. Hill, L. Perelman, and C. Heisey (1997b), A finite-volume, incompressible Navier-Stokes model for studies ocean on parallel computers, *J. Geophys. Res.*, *102*(C3), 5753–5766, doi:10.1029/96JC02775.

Meade, R. H., and K. O. Emery (1971), Sea level as affected by river runoff, Eastern United States, *Science*, *173*, 425–428, doi:10.1126/science.173.3995.425.

Mitchum, G. T. (2011), Sea level changes in the southeastern United States: Past, present, and future, report, 16 pp., Florida Climate Institute and SE Climate Consortium. [Available at FloridaClimateInstitute.org and SEClimate.org.]

National Geophysical Data Center (NGDC) (1988), Data Announcement 88-MGG-02, in *Digital Relief of the Surface of the Earth, NOAA*, Natl. Geophys. Data Cent., Boulder, Colo. [Available at http://www.ngdc.noaa.gov/mgg/global/etopo5.html.]

National Oceanic and Atmospheric Administration (NOAA) (2014), National Oceanic and Atmospheric Administration Center for Operational Oceanographic Products and Services, NOAA CO-OPS, Washington, D. C. [Available at tidesandcurrents.noaa.gov.]

National Oceanographic Data Center (NODC) (1994), *The National Oceanographic Data Center World Ocean Atlas 1994 (NODC_WOA94)*, NOAA/OAR/ESRL PSD, Boulder, Colo. [Available at http://www.esrl.noaa.gov/psd.]

Pugh, D. T., and P. L. Woodworth (2014), *Sea-level Science: Understanding Tides, Surges, Tsunamis and Mean Sea-Level Changes*, 408 pp., Cambridge Univ. Press, Cambridge.

Rossby, T., C. N. Flagg, K. Donohue, A. Sanchez-Franks, and J. Lillibridge (2014), On the long-term stability of Gulf Stream transport based on 20 years of direct measurements, *Geophys. Res. Lett.*, *41*, 114–120, doi:10.1002/2013GL058636.

Sallenger, A. H. Jr., K. S. Doran, and P. A. Howd (2012), Hotspot of accelerated sea-level rise on the Atlantic coast of North America, *Nat. Clim. Change*, *2*, 884–888, doi:10.1038/nclimate1597.

Sandstrom, H. (1980), On the wind-induced sea level changes on the Scotian Shelf, *J. Geophys. Res.*, *85*, 461–468, doi:10.1029/JC085iC01p00461.

Shearman, R. K., and S. J. Lentz (2010), Long-term sea surface temperature variability along the U.S. east coast, *J. Phys. Oceanogr.*, *40*, 1004–1017, doi:10.1175/2009JPO4300.1.

Smith, D. M., and J. M. Murphy (2007), An objective ocean temperature and salinity analysis using covariances from a global climate model, *J. Geophys. Res.*, *112*, C02022, doi:10.1029/2005JC003172.

Smith, P. C. (1983), Eddies and coastal interactions, in *Eddies in Marine Science*, edited by A. R. Robinson, pp. 446–480, Springer, Berlin.

Stewart, R. H. (2008), *Introduction to Physical Oceanography*, 345 pp. [Available at http://oceanworld.tamu.edu/.]

Sturges, W., and B. C. Douglas (2011), Wind effects on estimates of sea level rise, *J. Geophys. Res.*, *116*, C06008, doi:10.1029/2010JC006492.

Thompson, K. R. (1986), North Atlantic sea-level and circulation, *Geophys. J. R. Astron. Soc.*, *87*, 15–32, doi:10.1111/j.1365-246X.1986.tb04543.x.

Thompson, P. R., and G. T. Mitchum (2014), Coherent sea level variability on the North Atlantic western boundary, *J. Geophys. Res. Oceans*, *119*, 5676–5689, doi:10.1002/2014JC009999.

van der Schrier, G., S. L. Weber, S. S. Drijfhout, and J. A. Lowe (2004), Low-frequency Atlantic sea level variability, *Global Planet. Change*, *43*, 129–144, doi:10.1016/j.gloplacha.2004.03.001.

Vignudelli, S., A. Kostianoy, P. Cipollini, and J. Benveniste (Eds.) (2011), *Coastal Altimetry*, 565 pp., Springer, Berlin.

Wessel, P., and W. H. F. Smith (1998), New, improved version of Generic Mapping Tools released, *EOS Trans. AGU*, *79*, 579.

Williams, R. G., V. Roussenov, D. Smith, and M. S. Lozier (2014), Decadal evolution of ocean thermal anomalies in the North Atlantic: The effects of Ekman, overturning, and horizontal transport, *J. Clim.*, *27*, 698–719, doi:10.1175/JCLI-D-12-00234.1.

Woodworth, P. L. (2012), A note on the nodal tide in sea level records, *J. Coastal Res.*, *28*, 316–323, doi:10.2112/JCOASTRES-D-11A-00023.1.

Woodworth, P. L., W. R. Gehrels, and R. S. Nerem (2011a), Nineteenth and twentieth century changes in sea level, *Oceanography*, *24*, 80–93, doi:10.5670/oceanog.2011.29.

Woodworth, P. L., M. Menéndez, and W. R. Gehrels (2011b), Evidence for century-timescale acceleration in mean sea levels and for recent changes in extreme sea levels, *Surv. Geophys.*, *32*(4-5), 603–618 (erratum page 619), doi:10.1007/s10712-011-9112-8.

Yin, J., and P. B. Goddard (2013), Oceanic control of sea level rise patterns along the East Coast of the United States, *Geophys. Res. Lett.*, *40*, 5514–5520, doi:10.1002/2013GL057992.

Yin, J., M. E. Schlesinger, and R. J. Stouffer (2009), Model projections of rapid sea-level rise on the northeast coast of the United States, *Nat. Geosci.*, *2*, 262–266, doi:10.1038/ngeo462.

Zervas, C. (2009), Sea level variations of the United States 1854–2006, *Tech. Rep. NOS CO-OPS 053*, Natl. Oceanic and Atmos. Admin., Washington, D. C. [Available at www.tidesandcurrents.noaa.gov.]